A Novel Resonant Frequency Tracking Control for Linear Compressor Based on MRAS Method

Wei Xu, *Senior Member, IEEE*, Qizhe Wang, Xiang Li, Yi Liu, *Member, IEEE*, and Jianguo Zhu, *Senior Member, IEEE*

***Abstract*—To optimize the efficiency of the linear compressor, its operating frequency must be controlled equal to the system resonant frequency. The traditional resonant frequency tracking control algorithm relies on the steady state characteristics of the system, which suffers from slow convergence speed, low accuracy and slow system response. In order to solve these problems, a novel resonant frequency tracking control for linear compressor based on model reference adaptive system (MRAS) is proposed in this paper, and the parameter adaptive rate is derived by the Popov's hyperstability theory, so that the system resonant frequency can be directly calculated through the parameter adaptive rate. Furthermore, the traditional algorithm needs to calculate the piston stroke signal by integrating the back-EMF, which has the problem of integral drift. The algorithm proposed in this paper only needs the velocity signal, and the accuracy of the velocity calculation can be ensured by utilizing the self-adaptive band-pass filter (SABPF), thereby greatly improving the accuracy of the resonance frequency calculation. Simulation results verify the effectiveness of the proposed algorithm.**

***Index Terms*—linear compressor, linear oscillating motor (LOM), resonant frequency tracking control, model reference adaptive system (MRAS).**

I. INTRODUCTION

TRADITIONAL compressors are driven by rotary motors, in which the crank-shaft mechanism is utilized to convert rotational motion into the reciprocating motion of the piston. The efficiency of traditional compressors is low because it has large mechanical losses due to the crank-shaft mechanism. The linear compressors directly driven by linear oscillating motor (LOM) have attracted much attention in recent years. Because of directly removing the crank-shaft mechanism, not only the efficiency of linear compressor can be greatly improved, but also the noise and volume reduced significantly [1]-[8]. However, the mechanical system of linear compressor contains a resonant spring, in which the efficiency is related to the system operating frequency. The system characteristics derived by the phasor method indicate that when the operating frequency is equal to the system resonant frequency, the linear compressor reaches highest efficiency. Therefore, a resonant frequency tracking control strategy must be implemented in the control system.

In 2004, Tae-Won Chun with Busan University investigated the system characteristics of LOM [9]. He pointed out that when the system reaches resonant state, the phase angle between piston stroke and motor current is 90°. Inspired by this conclusion, several resonant frequency tracking control strategies based on the phase angel between piston stroke and motor current have been proposed in recent years [10]-12[]. The first step of these strategies is to obtain the piston stroke signal and the current signal, and then extract the phase angel through algorithm. Finally, a hysteresis controller is utilized to adjust the system operating frequency ensuring the phase angel reaches 90°. Therefore, these strategies are similar except that the phase angel detection algorithm is different. Some common detection algorithms are commented as follows: The zero-crossing detection algorithm is easy to implement, but it is sensitive to noise [10]; the fast Fourier transform algorithm with high accuracy needs expensive computation; the waveform fitting phase detection (WFPD) algorithm requires both large data storage space and massive computation [11]. In 2008, the average value of stroke-current product (ASCP) method with less computation was proposed, yet its calculation accuracy will decrease when the frequency changes [12]. Furthermore, hysteresis regulator is utilized to adjust the frequency since the phase angel and the frequency are not strictly proportional, leading to convergence difficulty. In addition, accurate phase angel can only be detected when the system reaches steady state, so the resonant frequency tracking control strategy cannot be implemented before the piston stroke reaches a steady state, which leads to slow system response.

In this paper, a novel resonant frequency tracking control strategy based on model reference adaptive system (MRAS) is proposed and investigated. The system equivalent spring coefficient and system equivalent damping coefficient are regarded as the adjustable parameters need to be identified. The electrical dynamics equation is regarded as the reference model, and the mechanical dynamics equation is regarded as the

Manuscript was submitted for review on 29, March, 2020.

This work was supported in part by the National Natural Science Foundation of China under Grants 51877093 and 51707079, in part by the National Key Research and Development Program of China under Grant 2018YFE0100200, and in part by the Key Technical Innovation Program of Hubei Province under Grant 2019AAA026.

Wei Xu, Qizhe Wang (Corresponding Author), Xiang Li, and Yi Liu are with the State Key Laboratory of Advanced Electromagnetic Engineering and Technology, School of Electrical and Electronic Engineering, Huazhong University of Science and Technology, Wuhan, 430074, China. (E-mails: weixu@hust.edu.cn; m201871463@hust.edu.cn; xiangl@hust.edu.cn; liuyi82@hust.edu.cn)

Jianguo Zhu is with the School of Electrical and Information Engineering, University of Sydney, Sydney, NSW 2006, Australia (E-mail: jianguo.zhu@sydney.edu.au).

Digital Object Identifier 10.30941/CESTEMS.2020.00028

adjustable model. The system resonant frequency can be directly calculated through the parameter adaptive rate derived by the Popov's hyperstability theory. Furthermore, only the velocity signal is required during the calculation, thus improving the calculation accuracy. Compared with the traditional resonant frequency tracking control algorithm, the proposed algorithm has advantages of high accuracy, fast convergence speed, fast system response speed, and so on.

II. System Characteristics Analysis And Traditional Control Strategy

A. System Model

The equivalent circuit diagram of linear compressor is shown in Fig. 1, the electrical dynamics equation can be written as

$$U = Ri + L\frac{di}{dt} + \alpha v \tag{1}$$

where U is the stator voltage, R the stator resistance, i the stator current, L the stator winding inductance, α the electromagnetic thrust constant, and v the piston velocity.

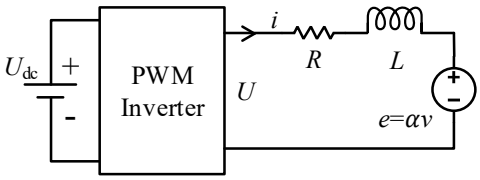

Fig. 1. Equivalent circuit of linear compressor.

Fig. 2 shows the simplified kinetic model of linear compressor, and the mechanical dynamics equation can be expressed as

$$m\frac{d^2x}{dt^2} + c_m\frac{dx}{dt} + k_m x + F_g = F_e = \alpha i \tag{2}$$

where m is the mass of piston, x the piston stroke, c_m the mechanical damping coefficient, k_m the mechanical spring coefficient, F_g the gas force, F_e the electromagnetic force.

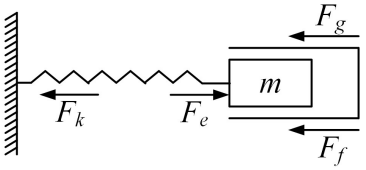

Fig. 2. Simplified kinetic model of linear compressor.

In order to analyze system characteristics, the non-linear gas forces F_g must be linearized. F_g can be expressed by utilizing the Describing Function Method, as illustrated by

$$F_g = k_g x + c_g v \tag{3}$$

where k_g is the equivalent gas spring coefficient, and c_g the equivalent gas damping coefficient.

By substituting (3) into (2), the linearized mechanical dynamics equation can be expressed as

$$m\frac{d^2x}{dt^2} + c\frac{dx}{dt} + kx = \alpha i \tag{4}$$

where c is the system equivalent damping coefficient, $c=c_m+c_g$, and k the system equivalent spring coefficient, $k=k_m+k_g$.

B. System Characteristics

As shown in Fig. 1, the linear compressor is powered by single phase inverter, so the stator current and voltage are both single phase AC quantities. Phasor method is generally used to analyze the characteristics of single-phase AC systems, (1) and (4) in frequency domain can be derived as follows, respectively:

$$\dot{U} = R\dot{I} + jwL\dot{I} + \alpha\dot{V} \tag{5}$$

$$-mw^2\dot{X} + jwc\dot{X} + k\dot{X} = \alpha\dot{I} \tag{6}$$

The relationship between voltage and current can be derived by substituting (6) into (5):

$$\dot{U} = \left[\left(R + jwL\right) + \frac{\alpha^2}{c + j(wm - k/w)}\right]\dot{I} \tag{7}$$

Then based on (7), the input power P_{in} can be calculated by

$$P_{in} = \mathrm{Re}(\dot{U}\dot{I}^*) = \left[\frac{\alpha^2 c}{c^2 + (mw - k/w)^2} + R\right]\left|\dot{I}\right|^2 \tag{8}$$

The output power of linear compressor P_{out} is defined as

$$P_{out} = \mathrm{Re}(F_g V^*) = \mathrm{Re}\left((c_g\dot{V} + k_g\dot{X})V^*\right) = c_g\dot{V}V^* \tag{9}$$

Generally, the efficiency is defined as the ratio of output power to input power. By substituting (6) into (9), P_{out} can be expressed as

$$(P_{out} = \frac{k_i^{\,2} c_g}{c^2 + (mw - k/w)^2}\left|\dot{I}\right|^2 \tag{10}$$

Thus, the efficiency can be derived as

$$\eta = \frac{P_{out}}{P_{in}} = \frac{\alpha^2 c_g}{\alpha^2 c + R\left[c^2 + (mw - k/w)^2\right]} \tag{11}$$

where w is the system operating frequency.

It can be seen from (11) that the system reaches maximum efficiency when operating frequency equals to the resonant frequency $\sqrt{k/m}$, and the resonance frequency will vary with the change of gas force since k_g is contained in k. Therefore, the resonant frequency tracking control strategy must be implemented to optimize the motor efficiency.

Furthermore, the phase angel between piston stroke and motor current under resonance can be derived from (6):

$$\dot{X} = \frac{\alpha}{(k - mw^2) + jwc}\dot{I} \tag{12}$$

$$\theta_{x-i} = -\arctan\left(\frac{wc}{k - mw^2}\right) \tag{13}$$

As can be seen from (13), when system reaches resonant state, the phase angle of piston stroke and motor current will equal 90°, which is the theoretical basis of the traditional resonant frequency tracking algorithm.

C. Traditional Resonant Frequency Tracking Algorithm

The key point of the traditional resonant frequency tracking control algorithm is the phase detection algorithm. Among various algorithms, the average value of stroke-current product (ASCP) algorithm that enjoys less computation is easy to implement. This section will briefly introduce this algorithm and the corresponding control system.

The piston stroke and motor current in steady state can be expressed as follows, respectively:

$$x = X\sin(wt) \tag{14}$$

$$i = I\sin(wt+\theta) \tag{15}$$

where θ is the phase angle between stroke and current.

The ASCP is defined as the average value of the product of the stroke and current, as illustrated by

$$\text{ASCP} = \frac{1}{T}\int_{t_0}^{t_0+T} x(t)\cdot i(t)dt = \frac{XI}{2}\cos\theta \tag{16}$$

Fig. 3 shows the relationships between the phase angle θ and ASCP, when the operating frequency is adjusted to equal to the resonant frequency, the phase angel θ becomes 90°, and consequently the value of ASCP is 0; when the operating frequency is higher than the resonance frequency, the angle θ is over 90◦, and the ASCP is negative. Therefore, the inverter frequency should be decreased to keep the ASCP at 0. Similarly, if the ASCP is positive, the inverter frequency should be increased.

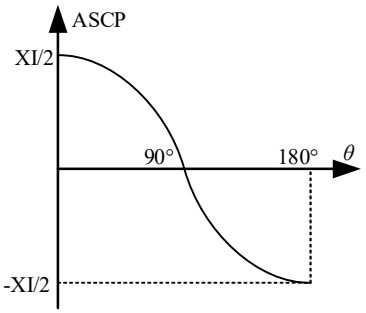

Fig. 3. Relation between the phase angle θ and ASCP.

The linear compressor control system based on the ASCP algorithm is shown in Fig. 4. The inverter frequency is adjusted by the hysteresis controller, ensuring the ASCP value equals to 0, and thus the resonant frequency tracking control can be achieved.

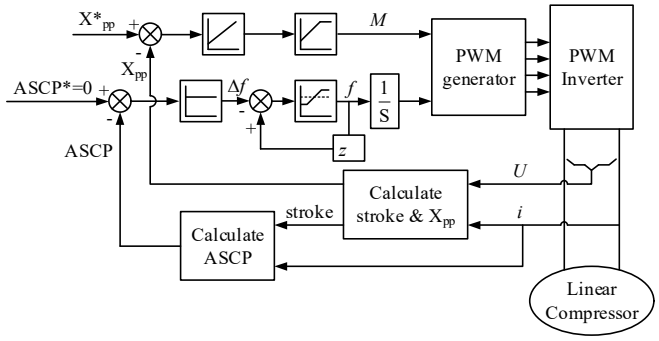

Fig. 4. Block diagram of the linear compressor control system.

In order to reduce costs and improve system reliability, the stroke signal required by the ASCP algorithm is provided by the back-EMF integration algorithm. The stroke signal can be calculated from voltage and current as follows:

$$x = \frac{1}{\alpha}\int (U - Ri - L\frac{di}{dt})dt \tag{17}$$

The pure integral term in (17) is generally replaced by a low-pass filter to avoid integral drift problem. However, the low-pass filter will inevitably cause the amplitude and phase deviations between calculated stroke and actual one. Obviously, if the stroke signal with phase deviation is provided to the resonance frequency tracking algorithm, the final resonance frequency tracking result will be inaccurate.

III. Novel Resonance Frequency Tracking Control Algorithm

A. Model Reference Adaptive System

To construct a MRAS parameter identification system, the first step is to determine the adjustable parameters that need to be identified. And then the system equations without the adjustable parameters are regarded as reference models, and the system equations with the adjustable parameters are regarded as adjustable models, and the output of these two models must have the same physical meaning. Finally, the output difference between these two models is input to the parameter adaptive mechanism, making the adjustable parameters be continuously adjusted by utilizing appropriate parameter adaptive rate. Hence, the outputs of these two models tend to be consistent, and the adjustable parameters equal to their actual values. Fig. 5 shows the structure of typical model reference adaptive system.

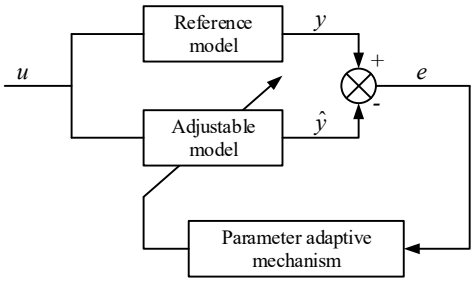

Fig. 5. The structure of typical model reference adaptive system.

The key point in designing a model reference adaptive system is to choose an appropriate parameter adaptive rate. At present, the most commonly used design method is based on Popov's superstability theory. This method first constructs an error system based on the selected adjustable model, and then converts the error system into a form consisting of a linear forward path and a non-linear feedback path as shown in Fig. 6.

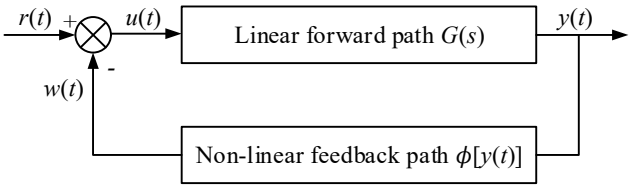

Fig. 6. The structure of typical model reference adaptive system.

According to Popov's hyperstability theory, if the input and output of the nonlinear feedback path satisfy Popov's integral inequality (18), the necessary and sufficient condition for the gradual stability of the entire system is that the transfer function of the linear forward path is strictly positive real (SPR).

$$\eta = \int_{t_0}^{t_1} w^T(t)y(t)dt \geq -\gamma_0^2 \quad (\forall t_1 > t_0, \gamma_0^2 \geq 0) \tag{18}$$

where w is the output of the nonlinear feedback path, y the input of the nonlinear feedback path, and γ_0 a constant.

For permanent magnet motors and induction motors, the adjustable parameter is generally the rotating velocity, which varies much slower than current. But as for linear oscillation motors, piston velocity and stroke are sinusoidal quantities with the same frequency as voltage and current. Therefore, as for linear oscillating motors, either velocity or stroke cannot be regarded as the adjustable parameters.

Based on the analysis in Section II, it can be seen that the parameters *k* and *c* are variables related to the gas force load. If the load is constant, *k* and *c* are constants and the parameter *k* is proportional to the square of the system resonance frequency. Therefore, *k* and *c* can be regarded as adjustable parameters to be identified. According to the selection principle of the reference model and the adjustable model, the electrical dynamics equation (1) can be regarded as the reference model, and its output represents the actual velocity; the mechanical dynamics equation (4) is regarded as the adjustable model, and its output represents the observed velocity.

B. Construction of Error System

To construct the error system shown in Fig. 6, (4) is rewritten as

$$pv = -\frac{k}{m}x - \frac{c}{m}v + \frac{\alpha}{m}i \tag{19}$$

where *p* is the differential operator.

To facilitate calculation, define parameters $K = -k/m$ and $C = -c/m$. Then express parameters and variables in (19) as estimated values and observed values, the adjustable model can be expressed as

$$p\hat{v} = \hat{K}\hat{x} + \hat{C}\hat{v} + \frac{\alpha}{m}i \tag{20}$$

where $\hat{v}$ is the observed velocity, $\hat{x}$ the observed piston stroke, $\hat{K}$ and $\hat{C}$ are estimated values of adjustable parameters.

The error equation is obtained by subtracting (19) from (20):

$$pe_v = Ke_x + Ce_v + (K-\hat{K})\hat{x} + (C-\hat{C})\hat{v} \tag{21}$$

where e_v is the velocity error, and e_x the stroke error.

According to the requirements of Popov's hyperstability theory, the error system should be converted into a form consisting of a linear forward path and a non-linear feedback path, so the error equation is rewritten as

$$pe_v = Ke_x + Ce_v - W \tag{22}$$

where $W = (\hat{K}-K)\hat{x} + (\hat{C}-C)\hat{v}$, W is the input of the linear forward path and the output of the non-linear feedback path. Defining the output of the linear forward path as $y=e_v$, the transfer function of the linear forward path can be derived according to (22).

The relationship between piston stroke and velocity is

$$px = v \quad p\hat{x} = \hat{v} \tag{23}$$

Therefore, the relationship between stroke error and velocity error is

$$pe_x = e_v \tag{24}$$

The s-domain form of (22) and (24) can be expressed as follows, respectively:

$$se_v(s) = Ke_x(s) + Ce_v(s) - W(s) \tag{25}$$

$$se_x(s) = e_v(s) \tag{26}$$

The transfer function of the linear forward path can be derived by substituting (26) into (25):

$$G(s) = \frac{e_v(s)}{-W(s)} = \frac{s}{s^2 - Cs - K} \tag{27}$$

Combing (20)-(27), the error system is established.

C. Parameter Adaptive Rate and System Stability

According to the error system constructed in the previous section, we substitute *W* and *y* into Popov's inequality (18):

$$\eta = \int_{t_0}^{t_1}\left[(\hat{K}-K)\hat{x} + (\hat{C}-C)\hat{v}\right]e_v dt \geq -\gamma_0^2 \tag{28}$$

Equation (28) can be decomposed into two inequalities as follows:

$$\eta_1 = \int_{t_0}^{t_1}(\hat{K}-K)\hat{x}e_v dt \geq -\gamma_1^2 \tag{29}$$

$$\eta_2 = \int_{t_0}^{t_1}(\hat{C}-C)\hat{v}e_v dt \geq -\gamma_2^2 \tag{30}$$

where γ_1 and γ_2 have the same meaning as γ_0.

The parameter adaptive rate is generally in the form of proportional integral, taking adaptive rate of *K* as an example:

$$\hat{K} = \int F_1(y,t,\tau)d\tau + F_2(y,t) + \hat{K}(0) \tag{31}$$

By substituting (31) into (29), the Popov's inequality is expressed as

$$\eta_1 = \int_{t_0}^{t_1}\left[\int F_1(y,t,\tau)d\tau + F_2(y,t) + \hat{K}(0) - K\right]\hat{x}e_v dt \geq -\gamma_1^2 \tag{32}$$

Equation (32) can also be decomposed into two inequalities as follows:

$$\eta_{11} = \int_{t_0}^{t_1}\left[\int F_1(y,t,\tau)d\tau + \hat{K}(0) - K\right]\hat{x}e_v dt \geq -\gamma_{11}^2 \tag{33}$$

$$\eta_{12} = \int_{t_0}^{t_1}F_2(y,t)\hat{x}e_v dt \geq -\gamma_{12}^2 \tag{34}$$

where γ_{11} and γ_{12} have the same meaning as γ_0.

To satisfy inequality (34), a function $f(t)$ that satisfies the following conditions is constructed:

$$\begin{cases} \dfrac{df(t)}{dt} = \hat{x}e_v \\ nf(t) = \int F_1(y,t,\tau)d\tau + \hat{K}(0) - K \end{cases} \tag{35}$$

where *n* is a constant and $n>0$.

By substituting (35) into (33), inequality (33) is derived as

$$\begin{aligned} \eta_{11} &= \int_{t_0}^{t_1} nf(t)df(t) \\ &= \frac{n}{2}\left[f^2(t_1) - f^2(t_0)\right] \geq -\frac{n}{2}f^2(t_0) \geq -\gamma_{11}^2 \end{aligned} \tag{36}$$

It can be seen that the constructed function $f(t)$ can satisfy inequality (33), and the expression of function F_1 can be obtained by deriving the second formula in (35):

$$F_1(y,t,\tau) = k_I\hat{x}e_v \quad (k_I > 0) \tag{37}$$

For inequality (34), if the integral term is regular, the inequality will obviously hold, and hence the function F_2 can be taken as

$$F_2(y,t) = k_P\hat{x}e_v \quad (k_P > 0) \tag{38}$$

The parameter adaptive rate of *K* can be obtained by substituting (37) and (38) into (31):

$$\hat{K} = k_p\hat{x}e_v + k_I\int\hat{x}e_v dt + \hat{K}(0) \tag{39}$$

The parameter adaptive rate of *C* can also be derived after similar derivation:

$$\hat{C} = k_p\hat{v}e_v + k_I\int\hat{v}e_v dt + \hat{C}(0) \tag{40}$$

The parameter adaptative rate specified by (39) and (40) can satisfy the Popov integral inequality. According to Popov's

hyperstability theory, the necessary and sufficient condition for the asymptotic stability of the entire system is that the transfer function of the linear forward path is a strictly positive real function. According to the definition of positive reality, if the following three conditions are met, the rational function $G(s) = N(s)/D(s)$ for the complex variable $s=\sigma+j\omega$ is a strictly positive real function:

(1) $G(s)$ is defined when s is real;

(2) $G(s)$ has no poles on the right half-closed plane;

(3) $\mathrm{Re}[G(jw)]>0$ when $-\infty<w<\infty$.

Condition (1) is obviously satisfied, and the poles of $G(s)$ are all on the left plane by utilizing the Routh Criterion, so Condition (2) is satisfied.

The transfer function $G(s)$ can be derived by substituting $s=jw$ into (27), as illustrated by

$$G(jw)=\frac{w^2\frac{c}{m}+jw(\frac{k}{m}-w^2)}{(\frac{k}{m}-w^2)^2+(w\frac{c}{m})^2} \tag{41}$$

The real part of $G(jw)$ is

$$\mathrm{Re}[G(jw)]=\frac{w^2\frac{c}{m}}{(\frac{k}{m}-w^2)^2+(w\frac{c}{m})^2} \tag{42}$$

From the physical meaning of the parameters, it is known that $c/m> 0$ and $k/m> 0$, so Condition (3) is satisfied.

According to the above proof, the constructed error feedback system satisfies Popov's hyperstability theory. So after that the corresponding signals are input to the parameter adaptive mechanism, the error between the reference model output and the adjustable model output will eventually converge to zero, which indicates the adjustable parameters will converge to their actual values.

D. Construction of Reference Models

The actual velocity can be calculated by (1):

$$v=\frac{1}{\alpha}(U-Ri-L\frac{di}{dt}) \tag{43}$$

Compare to (17), (43) does not contain pure integral term, so there is no integral drift problem. However, (43) contains a differential term for current, which will cause the noise in the current signal to be amplified. In order to solve this problem, a self-adaptive band-pass filter (SABPF) is used to obtain the fundamental component of the calculated velocity signal. Fig. 7 shows the structure diagram of SABPF.

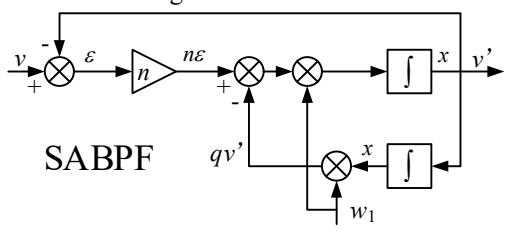

Fig. 7. Structure diagram of self-adaptive band-pass filter.

Overall, using (43) in combination with SABPF can achieve resonant frequency tracking control without a speed sensor. Compared with the ASCP method, the proposed algorithm estimates velocity rather than piston shift, so the accuracy of the proposed algorithm will suffer from neither integral drift error caused by the pure integral term, nor the amplitude and phase deviations caused by low-pass filter.

The transfer function between the output signal v' and the input signal v is:

$$D(s)=\frac{v'}{v}=\frac{nw_1s}{s^2+nw_1s+w_1^2} \tag{44}$$

where n is a constant, and w_1 the center frequency of SABPF.

Setting the center frequency w_1 = 100rad/s, then the Bode diagram of $D(s)$ at different values of n is shown in Fig. 8:

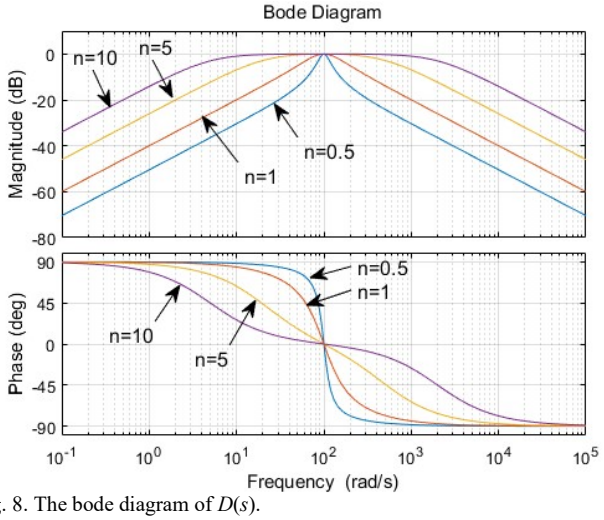

Fig. 8. The bode diagram of $D(s)$.

Fig. 8 illustrates that when the fundamental frequency w of the input signal v equals to the filter center frequency w_1, the output signal v' has no phase and amplitude offset from the input signal v, and the harmonics of other frequencies will be filtered. The parameter n is a scaling factor for adjusting the filtering bandwidth. Smaller n has better filtering effect, but the dynamic response speed will be slower. Since the frequency of velocity signal is same as the operating frequency of LOM, the center frequency of SABPF can be set equivalent to the system operating frequency, and then the harmonics caused by the derivative can be filtered without affecting the magnitude and phase of calculated velocity signal.

IV. Simulation Results

A. Control System and Startup Performance

To verify the effectiveness of the proposed algorithm, an LOA control system with the proposed algorithm is constructed in Matlab/Simulink as shown in Fig. 9.

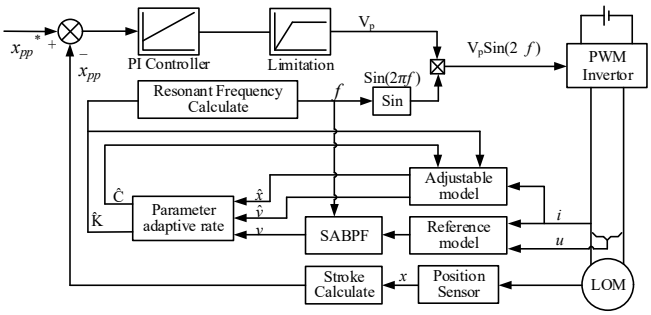

Fig. 9. Structure diagram of linear compressor control system.

The motor parameters in simulation are given as follows: the stator resistance is 18 Ω, the stator inductance 0.59 H, the thrust coefficient 47.08 N/A, the piston mass 0.93 kg, the system equivalent damping coefficient 20 N.s/m, and the system equivalent spring coefficient 30 kN/m, i.e. the system resonant frequency 28.59 Hz. The initial values of k and c are $k(0)$ = 20000 and $c(0)$ = 15, so that the initial values of K and C are $K(0)$ = 21505 and $C(0)$ = 16.13. In the startup process, the target amplitude is set to 5 mm, and the system startup frequency is 23.34 Hz, the parameters of PI controller are set to be: k_p=40, k_i=400 for stroke controller; k_p=500, k_i=60000 for K controller; k_p=5, k_i=500 for C Controller. In addition, in order to improve the accuracy of calculation and control, the original piston stroke signal is amplified by 1000 times.

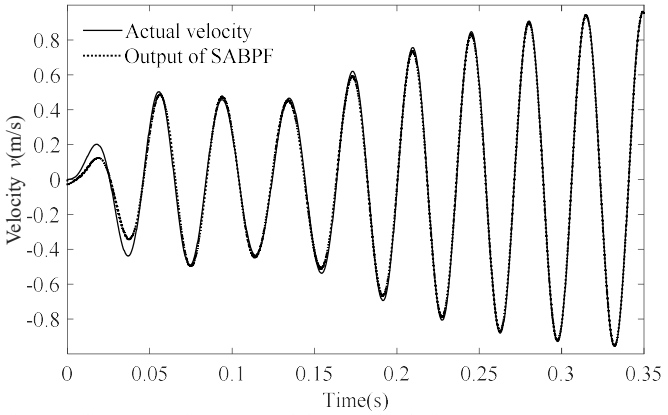

Fig. 10. The output of SABPF and the actual velocity

The center frequency of SABPF is set to be consistent with the system operating frequency as shown in Fig. 9, and the parameter n is set to 1.5. As shown in Fig. 10, the output of SABPF is almost the same as the actual speed after only one cycle. Therefore, the output of SABPF can be regarded as the output of the reference model, which represents the actual state of motor.

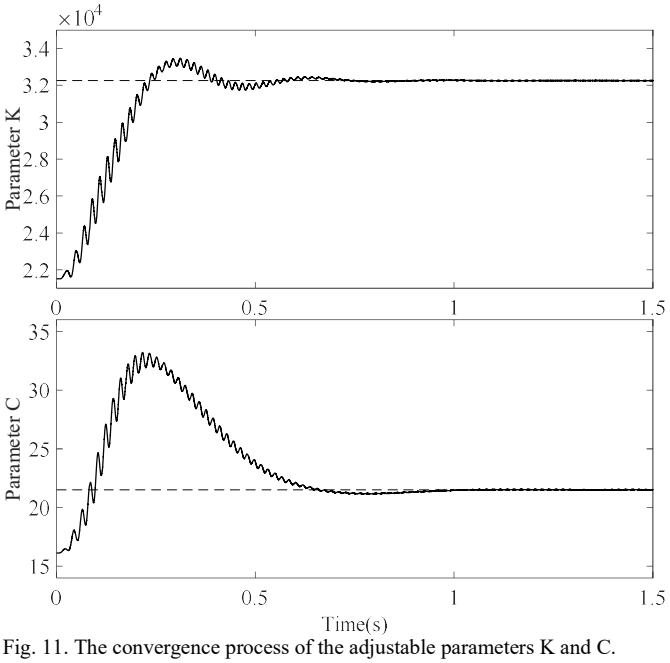

Fig. 11. The convergence process of the adjustable parameters K and C.

Fig. 11 shows the convergence process of the adjustable parameters K and C, the dotted lines represent the actual values of K and C, which are K = 30000/0.93 = 32258 and C = 20/0.93 = 21.51. It can be seen from Fig. 11 that the adjustable parameters K and C can quickly converge from the initial value to their actual values, and the ±1% settling time of K is about 0.5s, the ±1% settling time of C is about 0.7s.

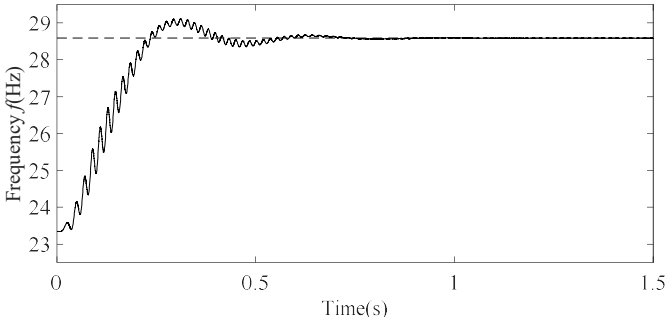

Fig. 12. Identification results of resonant frequency f.

Fig. 12 shows the identification results of resonant frequency f. The dotted lines represent the actual value of the system resonant frequency of 28.59 Hz. The parameter K is proportional to the square of the resonance frequency, so the convergence process of the resonance frequency and the parameter K is similar, and the ±1% settling time of f is also 0.5s. Fig. 11 and Fig. 12 illustrate the correctness of the derived parameter adaptive rate, demonstrating that the proposed algorithm has the advantages of fast convergence speed and high accuracy.

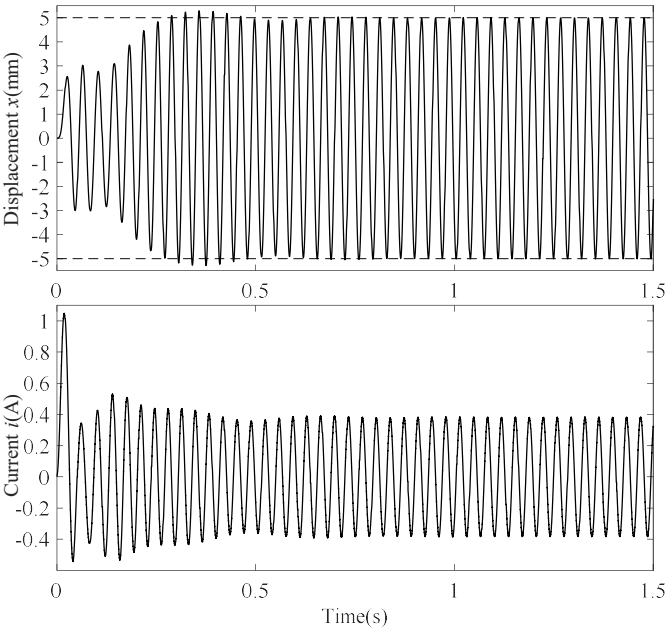

Fig. 13. Simulation results of piston stroke and motor current.

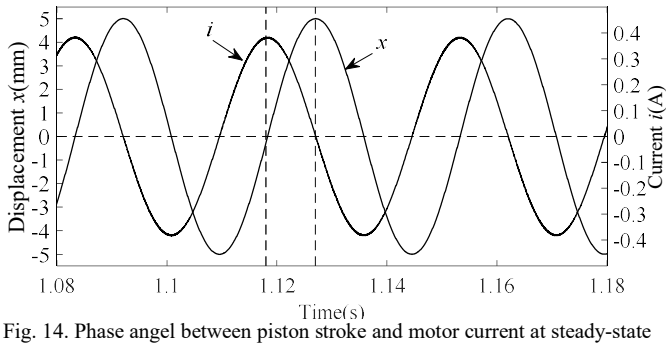

Fig. 14. Phase angel between piston stroke and motor current at steady-state

Figs. 13 and 14 show the variation of piston stroke and motor current during startup process, and the phase angel between piston stroke and motor current at steady-state, respectively. Under the calculation of the MRAS algorithm, the operating frequency quickly rises close to the system resonant frequency, that is, the stroke current ratio increases quickly, so the spike current only appears at the instant of startup. As shown in Fig. 13, under the adjustment of the stroke closed-loop controller, the stroke peak value quickly reaches a given value and the overshoot is small. Fig. 14 illustrates that the phase angle between piston stroke and motor current at steady state is 90°, which verifies the accuracy of the estimated resonance frequency from another aspect.

B. Response to Step Load Change

For linear compressors, a step load change means a sudden increase in the discharge pressure of the compressor. Several literatures indicate that the increase in the discharge pressure of linear compressors will cause the equivalent gas spring coefficient k_g and the equivalent gas damping coefficient c_g to increase. Therefore, the system equivalent spring coefficient k increases, and consequently the system resonance frequency goes up.

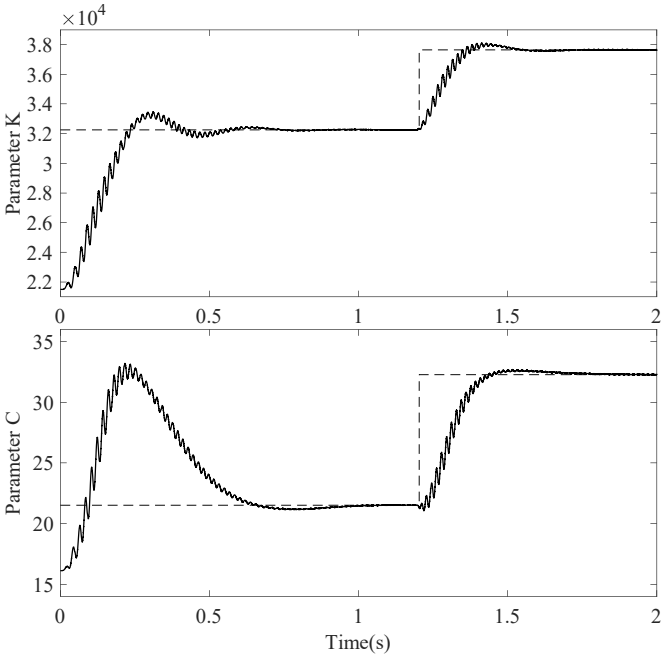

Fig. 15. Response of parameters K and C.

Fig. 15 shows the response to step load change. Before 1.2s, the system is in the startup state, and the relevant parameters are consistent with the previous section. At 1.2s, the system equivalent damping coefficient c increases from 20 to 30, and the system equivalent spring coefficient k increases from 30000 to 35000, so that the adjustable parameter C increases from 21.51 to 32.26, and parameter K increases from 32258 to 37634. It means the system resonant frequency increases from 28.59Hz to 30.88Hz. As shown in Fig. 15, the MRAS algorithm responds quickly after step load change, the adjustable parameters K and C quickly converge to the new actual values. The ±1% settling time of K and C is about 0.17s and 0.27s respectively.

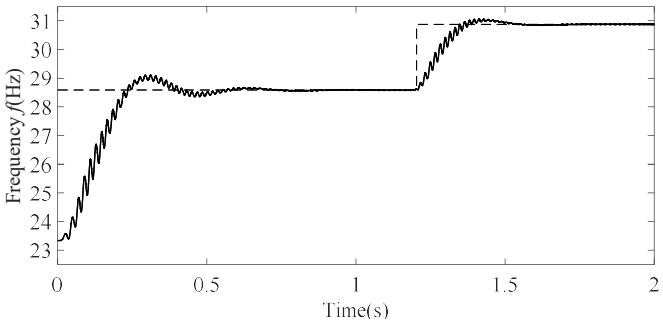

Fig. 16. Response of system resonant frequency.

Fig. 16 shows the response of system resonant frequency f, and the estimated value of the resonance frequency converges from 28.59Hz to the new actual value of 30.88Hz in 0.17s, which illustrate that the proposed MRAS algorithm has fast response speed and high convergence accuracy to step load change.

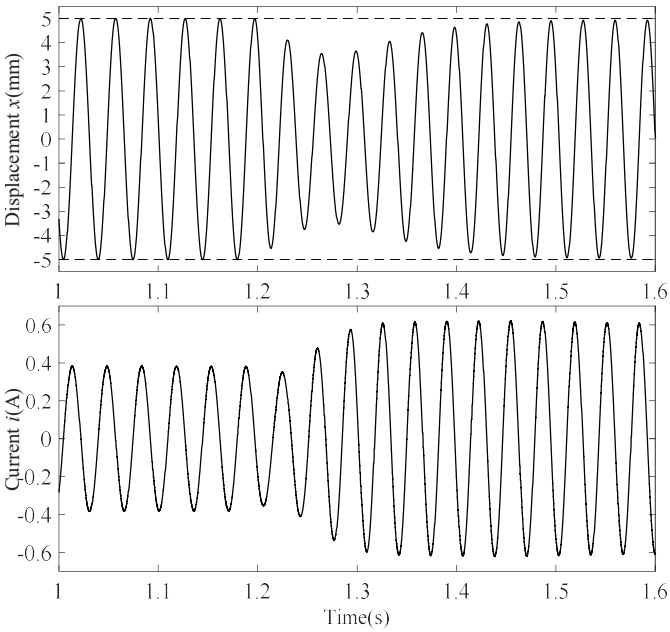

Fig. 17. Response of piston stroke and motor current.

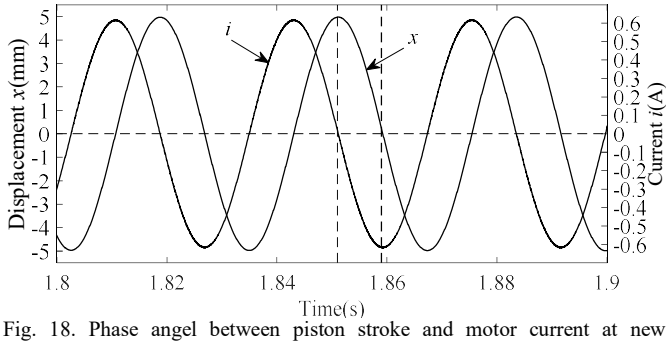

Fig. 18. Phase angel between piston stroke and motor current at new steady-state.

Fig. 17 shows the response of piston stroke and motor current. As seen from this figure, under the adjustment of the stroke closed-loop controller, the stroke amplitude reaches its given value after about 0.3s, and the current response is smooth without spike. Fig.18 illustrates that the phase angel between piston stroke and current at new steady-state is still 90°, which illustrates the new resonant frequency estimated by the MRAS algorithm is accurate.

C. Comparison with Traditional Algorithms

An LOM control system based on the ASCP algorithm is also constructed in Simulink so as to demonstrate the advantages of the proposed algorithm. The structure diagram of traditional linear compressor control system is shown in Fig. 4, and the motor parameters, operating conditions settings and the PI parameters of the closed-loop stroke controller are same as the previous section.

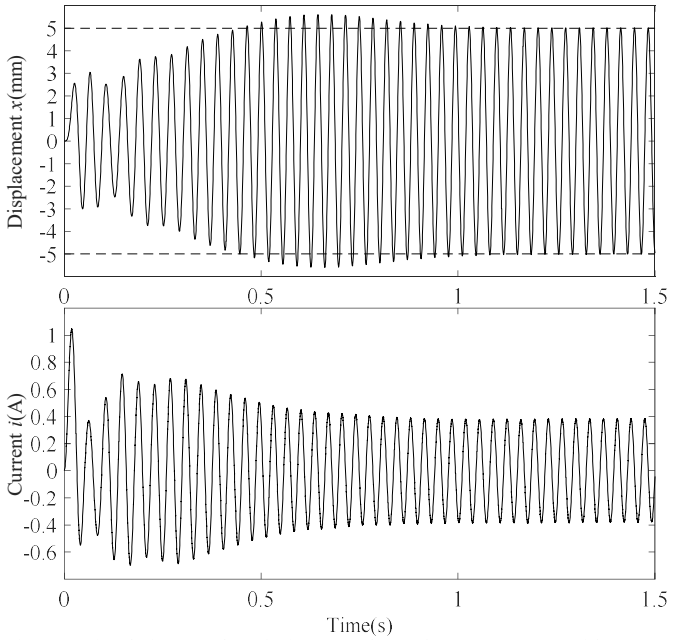

Fig. 19. Simulation results of piston stroke and motor current with ASCP algorithm under the first type of operating condition.

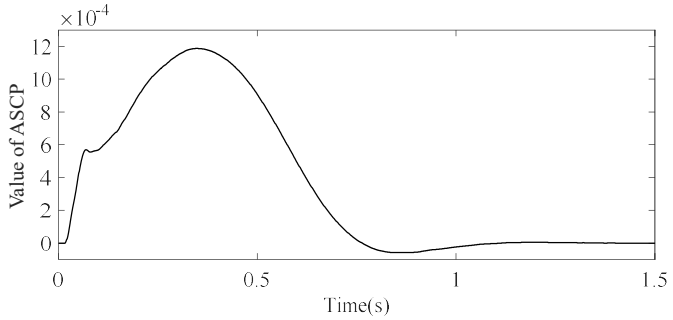

Fig. 20. The value of ASCP under the first type of operating condition.

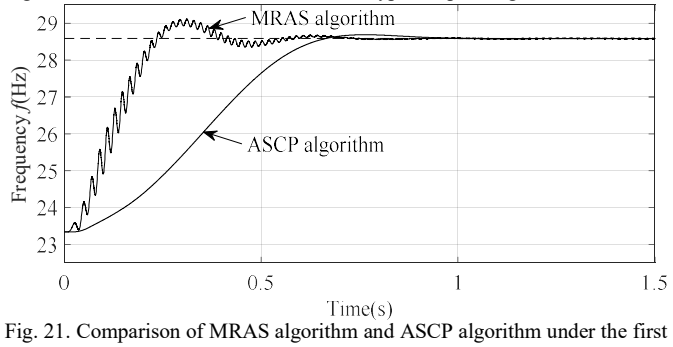

Fig. 21. Comparison of MRAS algorithm and ASCP algorithm under the first type of operating condition

Figs. 19-21 show the first type of operating condition, the ASCP algorithm starts to adjust the frequency at the beginning of the simulation. Fig. 21 illustrates that the MRAS algorithm has faster convergence speed compared with the ASCP algorithm under this operating condition. The reason for the slow convergence speed of the ASCP algorithm is that the algorithm uses the ASCP value as a reference for frequency adjustment. When the ASCP value is large, the operating frequency and the resonance frequency are considered to be quite different, and the frequency adjustment rate should be increased. On the contrary, if the ASCP value is small, the operating frequency at this time is considered to be very close to the resonance frequency, and the frequency adjustment rate should be reduced. However, the ASCP value is not only related to the phase angle between piston stroke and motor current, but also related to the product of stroke peak and current peak, according to (16). Therefore, when the motor is just started, the piston stroke and motor current have not reached their steady state, and the ASCP value is very small. Therefore, a lower frequency adjustment rate is adopted, which causes the algorithm to converge slowly, as shown in Figs. 19 and 20, respectively.

Figs. 22-24 show the second type of operating condition, in which the ASCP algorithm does not start until stroke and current reach steady state. As shown in Figs. 22 and 23, after that the stroke and current reach steady state, the ASCP value is basically stable and much larger than when the motor starts. Therefore, a higher frequency adjustment rate is adopted, as shown in Fig. 24, the ASCP algorithm has slightly slower convergence speed than MRAS algorithm.

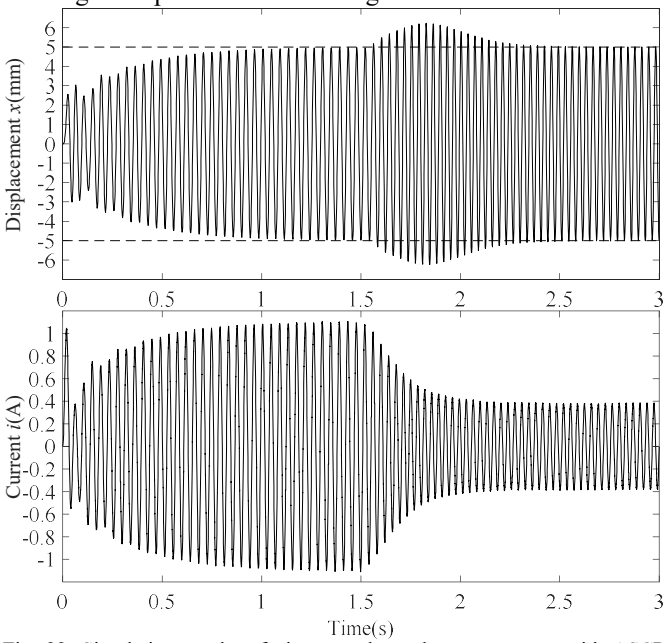

Fig. 22. Simulation results of piston stroke and motor current with ASCP algorithm under the second type of operating condition.

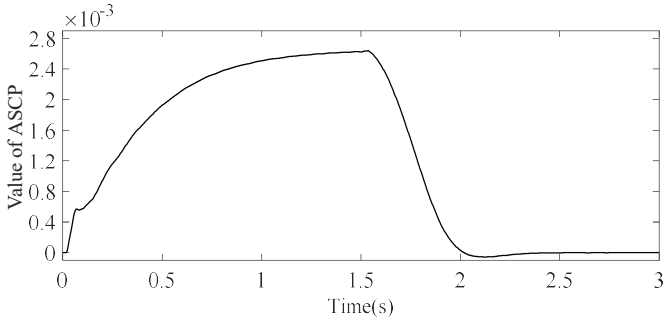

Fig. 23. The value of ASCP under the second type of operating condition.

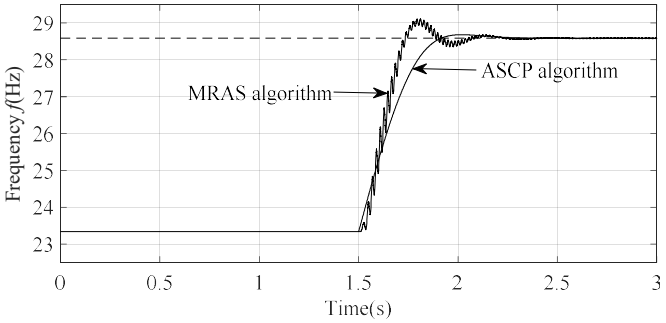

Fig. 24. The value of ASCP under the second type of operating condition.

However, in this operating condition, the frequency cannot be adjusted when the stroke is in a dynamic process, so the response speed of the whole system is greatly reduced.

V. CONCLUSION

In this paper, a novel resonant tracking control strategy for linear compressor based on MRAS is proposed and investigated. The electrical dynamics equation is regarded as the reference model, and the mechanical dynamics equation is regarded as the adjustable model, of which the parameter adaptive rate and system stability are proved by Popov's hyperstability theory. Simulation results have verified the correctness of the derived parameter adaptive rate. Moreover, comparative simulation results with traditional algorithms indicate that the proposed control strategy takes into account both the convergence speed of the algorithm and the response speed of the system, so that the whole system has demonstrated better performance.

REFERENCES

[1] X. Li, W. Xu, C. Ye, and I. Boldea, "Comparative study of transversal-flux permanent magnetic linear oscillatory machines for compressor," *IEEE Trans. Ind. Electron.,* vol.65, no.9, pp.7437-7446, Sep. 2018.

[2] X. Li, W. Xu, C. Ye, and J. Zhu, "Novel hybrid-flux-path moving-iron linear oscillatory machine with magnets on stator," *IEEE Trans. Magn.,* vol. 53, no.11, Article # 8210405, Nov. 2017.

[3] H. Lee, S. Ki, J. Kang, et al, "Noise characteristics of linear compressor for refrigerators," in *Proceeding of 15th International Conference on Sound and Vibration*, Daejeon, Korea, pp. 2714-2719, 2008.

[4] B. Hur, H. Lee, "Linear compressor," USA, US6398523B1. 2002-6-4.

[5] H. Lee, "Linear compressor," USA, US20080226473. 2008-09-18.

[6] K. Liang, "A review of linear compressors for refrigeration," *International Journal of Refrigeration*, vol. 84, pp. 253-273, Dec. 2017.

[7] H. Kim, C. Roh, J. Kim, J. Shin, Y. Hwang, J. Lee, "An experimental and numerical study on dynamic characteristic of linear compressor in refrigeration system," *International Journal of Refrigeration*, vol. 32, no. 7, pp. 1536–1543, Nov. 2009.

[8] W. Xu, X. Li, J. Zhu, and Q. Wang, "3D modelling and testing of a stator-magnet transverse-flux linear oscillatory machine for direct compressor drive," IEEE Transactions on Industrial Electronics, 2020, early access.

[9] Tae-Won Chun, Jung-Ryol Ann, Jae-Yoo Yoo and Chel-Woong Lee, "Analysis and control for linear compressor system driven by PWM inverter," *30th Annual Conference of IEEE Industrial Electronics Society, 2004. IECON 2004*, Busan, South Korea, 2004, pp. 263-267 Vol. 1.

[10] C. Demoulias and K. Gouramanis, "Voltage multiple-zero-crossings at buses feeding large triac-controlled loads," *IEEE Trans. Ind. Electron.*, vol. 54, no. 5, pp. 2853–2863, Oct. 2007.

[11] T. Zhang and H. Yu, "A novel strategy of resonant frequency tracking control for linear compressor," *2017 20th International Conference on Electrical Machines and Systems (ICEMS)*, Sydney, NSW, 2017, pp. 1-6.

[12] T. Chun, J. Ahn, H. Lee, H. Kim and E. Nho, "A novel strategy of efficiency control for a linear compressor system driven by a PWM inverter," *IEEE Trans. Ind. Electron.*, vol. 55, no. 1, pp. 296-301, Jan. 2008.

[13] J. Latham, M. L. McIntyre and M. Mohebbi, "Sensorless Resonance Tracking and Stroke Control of a Linear Vapor Compressor Via Nonlinear Observers," *IEEE Trans. Ind. Electron.*, vol. 65, no. 5, pp. 3720-3729, May. 2018.

[14] J. Latham, M. L. McIntyre and M. Mohebbi, "Paramete estimation and a series of nonlinear observers for the system dynamics of a linear vapor compressor," *IEEE Trans. Ind. Electron.*, vol. 63, no. 11, pp. 6736-6744, Nov. 2016.

[15] G. Yang and T. -. Chin, "Adaptive-speed identification scheme for a vector-controlled speed sensorless inverter-induction motor drive," *IEEE Trans. Ind. Appl.*, vol. 29, no. 4, pp. 820-825, July-Aug. 1993.

[16] H. Kubota, K. Matsuse and T. Nakano, "DSP-based speed adaptive flux observer of induction motor," *IEEE Trans. Ind. Appl*, vol. 29, no. 2, pp. 344-348, March-April 1993.

[17] M. S. Zaky, "Stability Analysis of Speed and Stator Resistance Estimators for Sensorless Induction Motor Drives," *IEEE Trans. Ind. Appl.*, vol. 59, no. 2, pp. 858-870, Feb. 2012.

[18] Y. Jiang, W. Xu, C. Mu, J. Zhu, and R. Dian, "An improved third-order generalized integral flux observer for sensorless drive of PMSMs," IEEE Transactions on Industrial Electronics, vol.66, no.12, pp. 9149 – 9160, Dec. 2019.

[19] W. Xu, Y. Jiang, C. Mu, and F. Blaabjerg, "Improved nonlinear flux observer based second-order SOIFO for PMSM sensorless control," IEEE Transactions on Power Electronics, vol. 34, no.1, pp.565-579, Jan. 2019.

[20] Y. Jiang, W. Xu, C. Mu, and Y. Liu, "Improved deadbeat predictive current control combined sliding mode strategy for PMSM drive system," IEEE Transactions on Vehicular Technology, vol. 67, no. 1, pp. 251-263, Jan. 2018.

Wei Xu (M'09-SM'13) received the double B.E. and M.E. degrees from Tianjin University, Tianjin, China, in 2002 and 2005, and the Ph.D. from the Institute of Electrical Engineering, Chinese Academy of Sciences, in 2008, respectively, all in electrical engineering. His research topics mainly cover design and control of linear/rotary machines.

From 2008 to 2012, he made Postdoctoral Fellow with University of Technology Sydney, Vice Chancellor Research Fellow with Royal Melbourne Institute of Technology, Japan Science Promotion Society Invitation Fellow with Meiji University, respectively. Since 2013, he has been Full Professor with State Key Laboratory of Advanced Electromagnetic Engineering in Huazhong University of Science and Technology, China. He has more than 100 papers accepted or published in IEEE Transactions Journals, two edited books published by Springer Press, one monograph published by China Machine Press, and more than 120 Invention Patents granted or pending, all in the related fields of electrical machines and drives. He is Fellow of the Institute of Engineering and Technology (IET). He will serve as the General Chair for 2021 International Symposium on Linear Drives for Industry Applications (LDIA 2021) and 2023 IEEE International Conference on Predictive Control of Electrical

Drives and Power Electronics (PRECEDE 2023), in Wuhan, China, respectively. He has served as Associate Editor for several IEEE Transactions Journals, such as IEEE Transactions on Industrial Electronics, and so on.

Qizhe Wang received the B.S. degree in electrical engineering from Huazhong University of Science and Technology, Wuhan, China, in 2018. He is currently working toward the M.S. degree in the School of Electrical and Electronic Engineering, Huazhong University of Science and Technology, Wuhan.

His research interests include advanced control methods for linear oscillating motor.

Xiang Li received the B.E. degree from Northwestern Polytechnical University, Xi'an, China, in 2015，the M.E. degree from Huazhong University of Science and Technology, Wuhan, China, in 2018. He is currently working toward the Ph.D. degree at the State Key Laboratory of Advanced Electromagnetic Engineering and Technology, Huazhong University of Science and Technology, Wuhan, China.

His research interests include design and analysis of novel permanent-magnet brushless machines.

Yi Liu (M'14) received his B.E. and M.E. degrees in Automation and Control Engineering from the Wuhan University of Science and Technology, Wuhan, China, in 2004 and 2007, respectively; and his Ph.D. degree in Mechatronic Engineering from the Huazhong University of Science and Technology, Wuhan, China, in 2016.

From 2007 to 2011, he was a Lecturer at the City College, Wuhan University of Science and Technology, Wuhan, China. From March 2016 to June 2016, he was a Senior R & D Engineer at the Fourth Academy of China Aerospace Science and Industry Group, Wuhan, China. In July 2016, he became a Postdoctoral Research Fellow at the State Key Laboratory of Advanced Electromagnetic Engineering and Technology, School of Electrical and Electronic Engineering, Huazhong University of Science and Technology.

His current research interests include AC electrical machine control and inverter systems.

Jianguo Zhu (S'93–M'96–SM'03) received the B.E. degree in 1982 from Jiangsu Institute of Technology, Jiangsu, China, the M.E. degree in 1987 from Shanghai University of Technology, Shanghai, China, and the Ph.D. degree in 1995 from the University of Technology Sydney (UTS), Sydney, Australia, all in electrical engineering. He was appointed a lecturer at UTS in 1994 and promoted to full professor in 2004 and Distinguished Professor of Electrical Engineering in 2017. In 2018, he joined the University of Sydney, Australia, as a full professor and Head of School for School of Electrical and Information Engineering.

His research interests include computational electromagnetics, measurement and modelling of magnetic properties of materials, electrical machines and drives, power electronics, renewable energy systems and smart micro grids.